Proc. Natl. Acad. Sci. USA
Vol. 95, pp. 14173–14178, November 1998
Cell Biology

Nucleosomes, linker DNA, and linker histone form a unique structural motif that directs the higher-order folding and compaction of chromatin

JAN BEDNAR*, RACHEL A. HOROWITZ*, SERGEI A. GRIGORYEV*, LENNY M. CARRUTHERS†, JEFFREY C. HANSEN†, ABRAHAM J. KOSTER‡, AND CHRISTOPHER L. WOODCOCK*§

*Department of Biology, University of Massachusetts, Amherst, MA 01003; ‡Department of Molecular Structural Biology, Max Planck Institute for Biochemistry, 8033 Martinsried, Germany; and †Department of Biochemistry, The University of Texas Health Sciences Center, 77303 Floyd Curl Drive, San Antonio, TX 78284

Communicated by K. E. van Holde, Oregon State University, Corvallis, OR, October 5, 1998 (received for review July 9, 1998)

ABSTRACT **The compaction level of arrays of nucleosomes may be understood in terms of the balance between the self-repulsion of DNA (principally linker DNA) and countering factors including the ionic strength and composition of the medium, the highly basic N termini of the core histones, and linker histones. However, the structural principles that come into play during the transition from a loose chain of nucleosomes to a compact 30-nm chromatin fiber have been difficult to establish, and the arrangement of nucleosomes and linker DNA in condensed chromatin fibers has never been fully resolved. Based on images of the solution conformation of native chromatin and fully defined chromatin arrays obtained by electron cryomicroscopy, we report a linker histone-dependent architectural motif beyond the level of the nucleosome core particle that takes the form of a stem-like organization of the entering and exiting linker DNA segments. DNA completes ≈1.7 turns on the histone octamer in the presence and absence of linker histone. When linker histone is present, the two linker DNA segments become juxtaposed ≈8 nm from the nucleosome center and remain apposed for 3–5 nm before diverging. We propose that this stem motif directs the arrangement of nucleosomes and linker DNA within the chromatin fiber, establishing a unique three-dimensional zigzag folding pattern that is conserved during compaction. Such an arrangement with peripherally arranged nucleosomes and internal linker DNA segments is fully consistent with observations in intact nuclei and also allows dramatic changes in compaction level to occur without a concomitant change in topology.**

Within the long arrays of nucleosomes that constitute the chromatin of most eukaryotic cells, the most thoroughly studied component is the nucleosome core particle, consisting of 145 bp of DNA wound on an octamer of "core" histones. Linker DNA interconnects core particles, varies in length depending on species and tissue, and usually is associated with the H1 class of "linker" histone (1, 2). Arrays of nucleosomes containing linker histone tend to form irregular fibers ≈30 nm in diameter (3), whose architecture and mode of compaction have been matters of controversy for almost 20 years (4–7). The controversy centers not on the structure of the nucleosome core particle, which has been solved at atomic resolution (8, 9), but on the arrangement and interactions of cores in three-dimensional (3D) space and the locations of linker DNA and linker histones (5, 6). The recent accumulation of evidence that chromatin structure above the level of the core particle plays a key role in determining the transcriptional status of genes and genetic loci (7, 10–19) illustrates the critical importance of understanding the fundamental folding properties of nucleosome arrays.

Studies of chromatin compaction in response to changes in the ionic environment (20) have established that the phenomenon can be accounted for by electrostatic interactions between DNA, histone proteins, and free ions (21). Major contributions to these interactions are provided by the N-terminal domains of the core histones, which contain ≈50% of the basic amino acids of the octamer (1, 9), and the C-terminal domains of the linker histones, which contain ≈60% of the positive charges in these molecules (1). Indeed, chromatin compaction requires the presence of the core histone N termini (22–24), and 30-nm chromatin fibers are not formed in the absence of linker histones (e.g., refs. 3 and 26). However, the precise interactions that lead to specific chromatin higher-order structures have remained elusive.

We have examined the folding and compaction of native chromatin fibers and fully defined, reconstituted nucleosomal arrays using electron cryomicroscopy (EC-M). EC-M has the advantage that it provides a snapshot of the solution conformation of unfixed, unstained specimens, and has been applied successfully to many macromolecular assemblies that have been inaccessible to more conventional microscopy techniques (27, 28). High-resolution EC-M images now have provided new insights into the detailed arrangement of linker DNA as it enters and exits the nucleosome, and the dramatic organizing influence of linker histone in this region. By including fully defined chromatin arrays in these EC-M studies, it is possible to go beyond the analysis of "random sequence" chromatin and correlate chromatin structure with sedimentation properties under identical solution conditions. The data suggest that the interactions of linker DNA and linker histone result in a unique structural motif that directs chromatin folding and compaction.

MATERIALS AND METHODS

Preparation of chicken erythrocyte chromatin, EC-M, and image processing were as described (29), except that for long chromatin fibers, nuclei were digested using 1 unit micrococcal nuclease per 50 μg DNA in 60 mM KCl/15 mM NaCl/15 mM Pipes, pH 7.8/0.3 mM $MgCl_2$/0.3 mM $CaCl_2$/0.1 mM phenylmethylsulfonyl fluoride (PMSF), for 45 min at 4°C, then 30 sec at 37°C. The reaction was stopped with EDTA, soluble chromatin was collected after 1 hr on ice, and dialyzed against 5 mM NaCl/10 mM Pipes/0.1 mM EDTA. COS-7 cells were grown in DMEM, and nuclei were isolated by Nonidet P-40 lysis in RSB (10 mM NaCl/3 mM $MgCl_2$/1 mM PMSF/10 mM Tris, pH 7.5) and digested with micrococcal nuclease in RSB plus 1 mM $CaCl_2$. Defined chromatin arrays were produced on DNA containing six tandem repeats of a 208-bp rDNA se-

The publication costs of this article were defrayed in part by page charge payment. This article must therefore be hereby marked "*advertisement*" in accordance with 18 U.S.C. §1734 solely to indicate this fact.

Abbreviations: EC-M, electron cryomicroscopy; EM, electron microscopy; 3D, three-dimensional.

§To whom reprint requests should be addressed. e-mail: chris@bio.umass.edu.

quence of *Lytechinus variegatus* (30) using salt dialysis (31, 32). For H5-containing arrays, the dialysis was stopped at 0.5 M NaCl, with 1.2 mol H5 added per mole of 208-bp repeat, held on ice for 3 hr, then dialyzed to 2.5 mM NaCl/0.25 mM EDTA/10 mM Tris, pH 7.8. Native oligonucleosomes (n = ≈5–7) were prepared from chicken erythrocyte chromatin as described (29). For ECM, a 3-μl drop of specimen at ≈50 μg/ml was applied to a grid covered with a perforated supporting film and mounted on a gravity-driven plunger enclosed in a humid chamber. Excess liquid was removed, leaving a 60- to 80-nm film of specimen, and the grid was plunged into liquid ethane, placed in a cryo holder (Gatan, Pleasanton, CA), and transferred to a Philips CM10 electron microscope. Low-dose stereo-pair images (separation, 30°) were recorded on Kodak SO163 film at 60 kV and ×46,000 direct magnification with ≈1-μm underfocus. Negatives were digitized by using a Hamamatsu TV camera with typical pixel size of 0.53 nm. To reduce the underfocus effect, a contrast transfer function (CTF) correction was applied (29, 33) with amplitude contrast contribution set to 12%, and the images were low-pass-filtered by using an ideal filter with the cutoff radius set to the position of the first zero of the CTF.

For cryotomography, oligonucleosomes from sucrose gradients (29) were adjusted to 80 mM NaCl, frozen hydrated preparations were made, and tilt images were recorded at a dose of 1.4e-/A^2 per image (34). The reconstruction shown in Fig. 3*b* was based on eight images with tilts distributed from −55° to +45°. Images were preprocessed with Weiner filtering according to the calculated contrast transfer function, with a data cutoff outside the first zero of the CTF. After inverse sinc-function weighting, the reconstructions were performed by back-projection. The validity of reconstructions of high-noise, limited data tilt series is discussed in ref. 34.

RESULTS AND DISCUSSION

Electron Cryomicroscopy as a Tool for Studying Chromatin Conformation. In EC-M, the sample in the chosen ionic environment is cryoimmobilized and then imaged in the frozen hydrated state. EC-M images thus provide snapshots of the solution conformation of freely diffusing chromatin arrays, and stereo or multiple tilt images allow 3D information to be retrieved. In the case of chromatin, the time to cryoimmobilization is crucial, since the helical repeat of DNA changes with temperature. Calculation suggests that cooling is too rapid to have a significant effect on DNA (27), and experiments using DNA sequences with a predicted degree of twist give the expected results (35). Moreover, both conventional electron microscopy (EM) and scanning-force microscopy of chromatin in low salt show a similar, basic zigzag structure as seen with EC-M (3, 36, 37). We therefore can be confident that the vitrification process preserves the solution conformation of chromatin samples.

The EC-M images shown here were obtained from chromatin released into solution by mild digestion of isolated chicken erythrocyte nuclei and also chromatin reconstituted onto DNA consisting of six tandemly arranged 208-bp units containing the nucleosome positioning sequence of the 5S rDNA of *Lytechinus variegatus* (30). When histone H5 was included, the reconstituted material behaved like native chromatin with respect to nuclease digestion and sedimentation (38) and proved to be morphologically indistinguishable from native oligonucleosomes (see below).

Linker Histones Induce a "Stem" Conformation of Linker DNA Segments. Fig. 1*a*, *b*, and *k* shows EC-M images of segments of unfixed, unstained chromatin fibers released from chicken erythrocyte nuclei into low-salt (≈5 mM M^+) buffer and observed in the frozen hydrated state. The fibers had a modal DNA length in excess of 10 kbp and contained equimolar amounts of core histones, as well as native levels of linker histones (not shown). Within the fibers, individual nucleosomes are seen in a variety of orientations and appear not as simple disks, but rather as pear-shaped structures connected by linker DNA that forms "stems" at the entry–exit sites similar to those observed in reconstituted mononucleosomes (39). Higher-resolution *en face* views of nucleosomes (Fig. 1 *f*, *g*, and *i*) show that linker segments typically leave the octamer tangentially after completing ≈1.7 turns on the histone octamer and subsequently continue on the same trajectory to an "intersection" zone about 8 nm from the nucleosome center, which extends for 3–5 nm, after which the two linker segments diverge. Viewed from the side (Fig. 1*h*), this zone is seen to be a region of close apposition of linker DNA, an arrangement that forms a distinctive, stem-like architectural motif.

Linker histones are required for the stem motif. In chromatin from which linker histones have been stripped, or in reconstituted nucleosomal arrays prepared with the core histones only (Fig. 1*c*), the length of DNA in contact with the histone core is unchanged (≈1.7 turns or 140–145 bp), but after leaving the core, the linker segments typically diverge from each other, as a result of their strong mutual repulsion, especially at low ionic strength (29, 40, 41). Representative scale models of nucleosomes illustrating potential linker DNA paths in the presence and absence of linker histones are shown in Fig. 3*d*, which includes three possible paths of linker DNA within the stem, each of which has different topological consequences (see below).

Close apposition of linker DNA segments in low-salt media requires screening of their mutual repulsion (21) and most probably is mediated by the C-terminal "tails" of linker histones, which contain ≈35 basic residues. An additional contribution from the N-terminal domains of histone H3 also appears likely (41). Interestingly, the length of the stem appears to be correlated with linker histone charge; chromatin containing H1 (Fig. 1*j*) generally having shorter stems than chromatin containing H5 (Fig. 1 *b*, *e*, and *k*). The stem motif is consistent with work demonstrating that the structured central domain of the linker histones binds near the linker DNA entry–exit region of the nucleosome (43, 44), and both the central and C-terminal domains are required for normal chromatin folding (26, 45). However, the precise locations of these histone domains within the stem structure remain to be determined.

The Structural Correlate of the Chromatosome. The EC-M images show that the amount of DNA wrapped around the histone octamer is similar (≈1.7 turns), both in the presence and absence of linker histone (Fig. 1). This suggests an explanation for the existence of the chromatosome, a short-lived, 166-bp intermediate in the generation of nucleosome core particles by micrococcal nuclease digestion (46). The chromatosome "pause" has been observed in native chromatin and in reconstituted chromatin containing either complete linker histone (47) or its structured domain only (26, 39). The 166 bp in the chromatosome has been attributed to the protection of two complete turns of DNA wrapped on the histone octamer, which would result in the entering and exiting DNA trajectories differing by 180°. In contrast, our observations indicate a completely different linker DNA path that arises from a wrapping of ≈1.7 turns of DNA on the octamer. This suggests that the chromatosome pause results from a protective interaction between linker histone and linker DNA, rather than between linker DNA and octamer, and that the equivalence of 166 bp and two turns of DNA wrapped on the histone octamer is coincidental.

The Low-Salt Solution Conformation of Chromatin Is a 3D Zigzag Fiber. EC-M images show that the low-salt solution conformation of native chromatin arrays is an irregular fiber, about 30 nm in diameter (Fig. 1 *a*, *b*, and *k*). A 3D reconstruction of a 9-nucleosome fiber segment, obtained from a tilt pair of micrographs in which the individual nucleosomes together with the stem conformation of the entering and exiting linker segments are represented by flattened, pear-

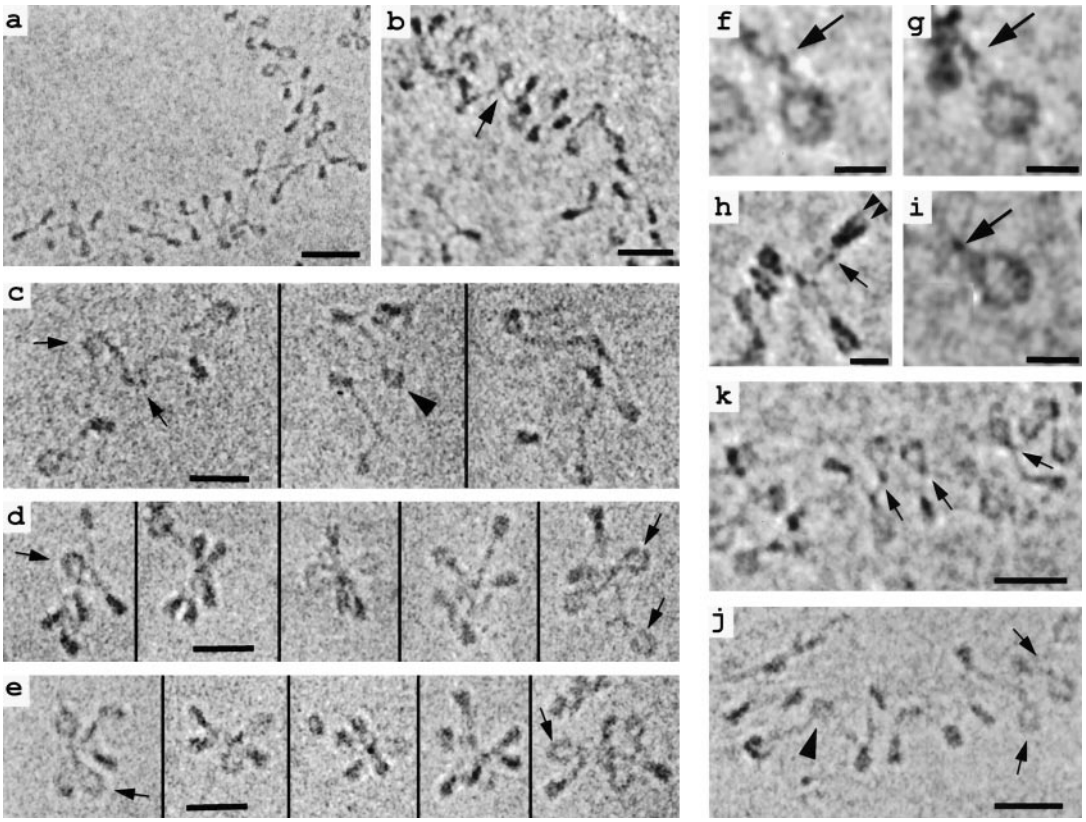

FIG. 1. (*a*, *b*, and *k*) Soluble chromatin from chicken erythrocyte nuclei vitrified in ≈5 mM M^+ and imaged unfixed and unstained in the frozen hydrated state. Nucleosomes and linker DNA are seen in many different orientations in these projections of the 3D structure. Arrows in *b* and *k* denote nucleosomes with the linker histone-dependent "stem" conformation described in the text. (*c*, *d*, and *f–i*) EC-M of unstained, unfixed chromatin reconstituted onto tandem DNA sequences containing the nucleosome-positioning sequence of 5S rDNA (30) and vitrified in 10 mM M^+. All samples except *c* contain linker histone H5. *En face* views of nucleosomes (*f*, *g*, and *i*) show the linker DNA entering and exiting the nucleosome tangentially, then "intersecting" and remaining apposed for 3–5 nm before diverging (arrows). Edge-on views (*h*) show the two gyres of DNA (arrowheads) and the apposition of linker DNA (arrow). (*c*) Reconstituted hexanucleosomes without histone H5. In most nucleosomes, the linker DNA segments diverge after leaving the histone core (arrows), but in some cases they appear to "cross over" (arrowhead). (*d*) Reconstituted hexanucleosomes as in *c*, but with added linker histone H5. The chromatin particles are more compact and adopt a star-like conformation in which "stem" structures are common (arrows). (*e*) EC-M images of small oligonucleosomes released from chicken erythrocyte nuclei after micrococcal nuclease digestion. A zigzag, star-like conformation is seen, and, like the reconstituted hexanucleosomes in *d*, linker DNA segments show the "stem" architecture (arrows). (*j*) Chromatin released from COS-7 cells and vitrified in 20 mM M^+ again shows a 3D zigzag conformation. While most nucleosomes show the stem motif (arrows), a few (arrowhead) have a linker DNA conformation typical of H1-free chromatin. [Bars = 10 nm (*f–i*); 30 nm for others.]

shaped solids, is shown in Fig. 3*a*. The stereo presentation clearly shows the 3D zigzag architecture (Fig. 3*a*) and illustrates that its construction may be viewed as a tandem arrangement of nucleosomes with the stem portions facing the interior of the fiber. The linker DNA segments are neither coiled nor do they conform to a simple zigzag (e.g., the model presented in ref. 52 and Fig. 3*c*), but rather are constrained within the stem motif. The constrained 3D zigzag and stem motif are ubiquitous in all chromatin samples we have examined, including random-sequence native chromatin released from chicken erythrocytes (Fig. 1 *a*, *b*, *e*, and *k*), chicken granulocytes, HeLa cells, COS-7 cells (Fig. 1*j*), and defined sequence chromatin reconstituted with core histone octamers and linker histone H5 (Fig. 1*d*). This ubiquity demonstrates that the stem architecture and 3D zigzag are not confined to the highly compact erythrocyte chromatin, which could be considered a special case, having more than one linker histone per nucleosome (48), the bulk of which consists of the strongly basic histone H5.

A 3D zigzag arrangement, dependent on linker histones (3, 29, 44), is consistent with the extensive literature on chromatin conformation at low ionic strength (reviewed in refs. 5 and 6) and, with various modifications, has featured in several chromatin fiber models (36, 37, 49–53). The organization of linker DNA segments into stem-like structures also is consistent with the ability of linker histones to prevent the mobility of positioned nucleosomes (54) and to inhibit transcription (e.g., refs. 44 and 55).

The Zigzag Arrangement Persists During Salt-Induced Compaction by Monovalent Ions (M^+). Chromatin fibers in solution are influenced strongly by the ionic environment (20), undergoing an approximately 5-fold compaction with relatively little change in diameter between 1 and 100 mM M^+ (56), and detailed sedimentation studies using defined nucleosomal arrays have shown that folding is continuous over this range (7, 57).

EC-M allows the compaction process to be followed much further than conventional EM and scanning-force microscopy, where resolution of nucleosomes and linker DNA becomes impossible at a very early stage (e.g., refs. 3, 36, 37, and 41). At ≈15 mM M^+, native chromatin fibers from chicken erythrocyte nuclei, which contain both H1 and H5, are already much more compact than at ≈5 mM (Fig. 2 *d* and *e*), and a similar level of compaction is reached at ≈40 mM with COS-7 cell chromatin (Fig. 2 *a–c*). The zigzag structure is retained, but the nearest neighbor nucleosomes are now much closer to each other, because of a systematic reduction in the linker DNA entry–exit angle of consecutive nucleosomes (29). For chicken erythrocyte chromatin, the mean 3D entry–exit angle changes from ≈85° (Fig. 1 *a–c*) to ≈45° (Fig. 2 *d* and *e*) over the 5–15 mM M^+ salt range. According to sedimentation studies, at 40

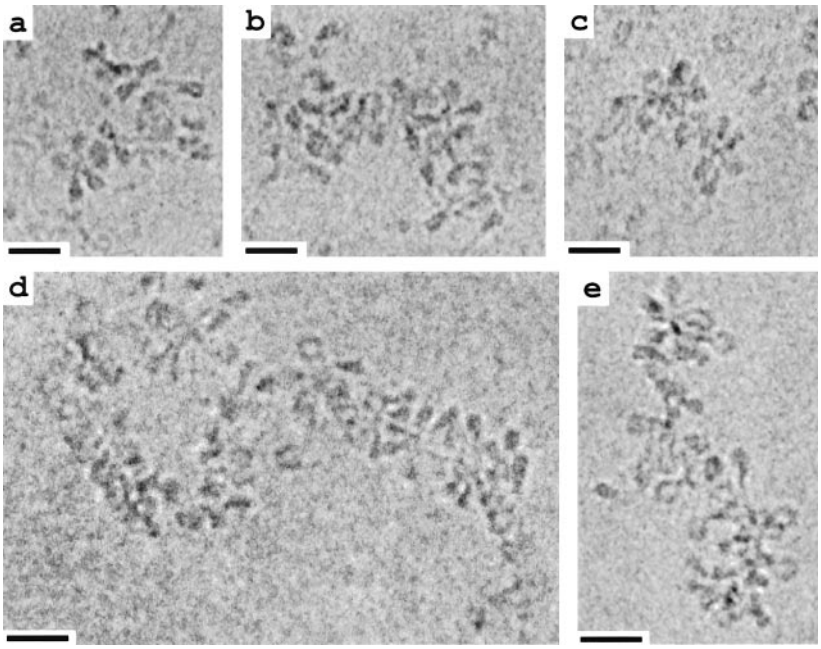

FIG. 2. EC-M of chromatin from COS-7 cells (*a–c*) vitrified in ≈40 mM ions and chicken erythrocyte nuclei (*d* and *e*) imaged in ≈15 mM ions. The fiber structure is consistent with an accordion-like compaction of the loose zigzags seen in Fig. 1. (Bar = 30 nm.)

mM M^+, defined chromatin arrays complete ≈80% of the maximal compaction obtainable with M^+ and ≈40% of the maximum compaction attainable with Mg^{2+} (31, 32, 38).

Since closer packing of nucleosomes makes it impossible to derive their 3D locations from tilt pairs of micrographs, we used electron cryotomography (34, 58) to follow the compaction process further. In reconstructions of several native chicken erythrocyte oligonucleosomes vitrified in 80 mM NaCl [higher salt concentrations induce their self-association (38)], it was possible to locate nucleosome positions and, in favorable cases, resolve linker DNA. A 3D model based on one of these reconstructions, in which 11-nm-diameter spheres are placed at the locations of nucleosomes, is shown as a stereo pair in Fig. 3*b* (in its present state of development, electron cryotomography does not provide sufficient detail of linker paths to identify stem structures). The chromatin forms an irregular 3D zigzag, with a mean linker DNA entry–exit angle of 34° (SD, 9°). All the reconstructions included a few instances, especially at the ends of the oligonucleosomes (Fig. 3*b*), of larger entry–exit angles. These cases, which greatly reduce the overall compaction level of the particles, probably represent nucleosomes lacking linker histone. Although the original projection images (not shown) suggested a very close packing of nucleosomes at this ionic strength, the 3D reconstructions reveal that individual nucleosomes generally do not touch under these conditions, as was also concluded from an electron cryotomographic study of long nucleosomal arrays obtained from erythrocyte nuclei of *Necturus maculatum* (34).

Higher-order chromatin folding is critically dependent on the N termini of the core histones (22–24, 41, 59). X-ray studies of nucleosome core particles show that these domains extend from the core particle and, for the most part, do not occupy fixed positions within the crystals (9). However, the molecular and structural details of their contribution to chromatin higher-order structures remain unclear. In the case of histone H4, the x-ray data indicate an interaction between one H4 N terminus and an acidic histone domain on the adjacent nucleosomal disk (9), which also could be relevant *in vivo*. It also has been pointed out that other N termini, especially those of H3, may contribute directly to the stem structure (41). Our EC-M data show that during the initial stages of the folding process, adjacent nucleosome disks remain separate and do not form close face-to-face contacts. Rather, compaction is produced through a reduction in linker DNA entry–exit angle (Table 1), suggesting a mechanism involving a strengthening of the stem motif.

Compaction Levels Observed Using EC-M Are Consistent with Other Biophysical Measurements. An important parameter of chromatin fibers related to the packing density of nucleosomes is the average mass per unit length. Since native fibers are irregular and mass per unit length is variable, we have used the mean linker entry–exit angles to construct models of zigzag chromatin that conform with the "average" EC-M observations, using principles discussed elsewhere (52). Fig. 3*c* shows models in which the linker entry–exit angles have been selected to match the angles measured for chicken erythrocyte chromatin at 5, 15, and 80 mM M^+ (the stem motif, omitted from these representations for simplicity, does not significantly influence the nucleosome packing ratio). To estimate the mass per unit length, the models were constructed with a fixed linker DNA length and entry–exit angle, but by varying these values, irregular fibers similar to those seen in the micrographs could be generated (52). The extent of compaction, presented as number of nucleosomes/11 nm of fiber (Table 1), agrees with the results of a detailed study using neutron-scattering and scanning-transmission EM with the same chromatin source and equivalent ionic conditions (56).

Conservation of Chromatin Fiber Architecture During Compaction. The two principal classes of proposals for the architecture of compact chromatin fibers share peripherally located nucleosomal disks, but diverge dramatically in other respects, including linker DNA path (reviewed in refs. 2 and 4–6). In solenoidal models, linker DNA is bent and continues the superhelical path established on the nucleosome core, allowing consecutive nucleosomes to come into close face-to-face contact with one another, while in zigzag models, the linker DNA segments are not coiled and consecutive nucleosomes are not nearest neighbors. That zigzag architectures fit the available data better than solenoidal structures has been reported by several authors. Staynov (49) examined possible arrangements of nucleosomes and linker DNA that satisfied existing experimental data and concluded that a zigzag structure best fit DNase I and II digestion patterns. Subsequently, Bordas *et al.* (50) adopted a regular zigzag as most compatible with their x-ray scattering data, and Williams *et al.* (51), on the

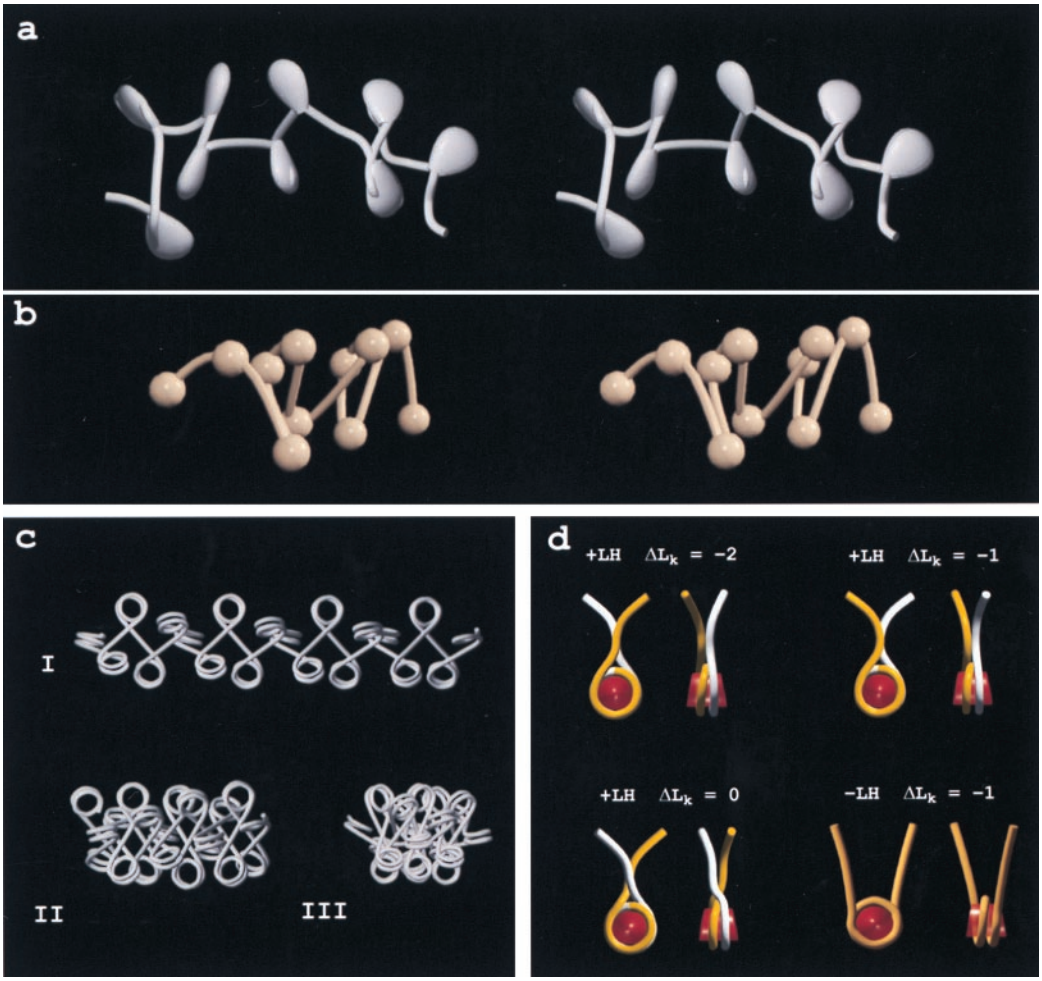

FIG. 3. (*a*) Stereo pair of a 3D model of a 9-nucleosome segment of a chicken erythrocyte chromatin fiber imaged in ≈5 mM M^+. Nucleosomes and their associated "stems" are represented by pear-shaped solids, all of which point toward the fiber interior. (*b*) Stereo pair of a chicken erythrocyte oligonucleosome vitrified in 80 mM M^+ and reconstructed from a tomographic tilt series. The quality of the reconstruction allowed nucleosome locations and linker paths to be identified, but details of nucleosome orientation and linker entry–exit sites were not resolved [Horowitz *et al.* (34)]. A movie of the reconstructed volume on which the model is based is available at http://www.ummed.edu/pub/r/rhorowit. (*c*) Models of uniform chromatin fibers based on principles discussed in Woodcock *et al.* (52), using the mean linker entry–exit angles measured from micrographs and reconstructions. Angles were 85° (I), 45° (II), and 34° (III). (*d*) Space-filling models of nucleosomes in the presence (+LH) and absence (−LH) of linker histones shown *en face* and in side views. With the stem conformation, differing linker paths, which appear to be energetically similar, result in differing linking numbers, ΔLk.

basis of x-ray and conventional EM data, introduced their helically symmetrical "crossed linker" model in which transverse linker segments cross the interior of the fiber. Also, Kubista *et al.* (53) reexamined earlier linear dichroism data and concluded that a zigzag, rather than solenoidal, arrangement was more consistent. More recently, zigzag arrangements that accommodate the observed structural irregularities in native chromatin fibers have been proposed (36, 52), and tomographic reconstructions of chromatin fibers in the nucleus also suggest an irregular zigzag conformation of nucleosomes and linker DNA *in situ* (60).

Table 1. Comparison of mass per unit length of chicken erythrocyte chromatin fibers predicted from EC-M images with neutron-scattering and scanning-transmission EM (STEM) measurements (56)

Ionic strength, (M^+)	Mean linker entry–exit angle from EC-M images	Mass per length from neutron-scattering and STEM data (56)	Mass per length from models based on EC-M data
5 mM	85°	1.5	1.6
15 mM	45°	3.2	3.0
80 mM	35°	6.0	5.9

The work presented here takes the evidence for a zigzag architecture a step further by providing direct evidence that the zigzag is not confined to the decondensed, low-salt conformation, but persists in the compact fiber. A transition from a low-salt zigzag architecture to a solenoidal conformation during compaction seems unlikely, given that it would require a substantial change in the trajectory of the linker DNA segments, especially at the nucleosome entry–exit sites where they are constrained by the linker histone-dependent stem structures. Rather, the present data suggest that linker DNA and linker histone contribute to the formation of a relatively rigid nucleosomal architecture, most likely promoted by electrostatic interactions, and this framework is the major determinant of chromatin fiber geometry and topology. During compaction, strengthening of the stem structures leads to a decrease in the linker entry–exit angle and an accordion-like reduction in fiber length.

It also should be noted that solenoidal models cannot readily accommodate the observed local variations in DNA linker length between nucleosomes (1) unless their lengths are strictly

"quantized" (61) or there is additional coiling of linker DNA (62). In solenoid-based chromatin fiber architectures, linker-length variations lead to changes in the location of the linker DNA entry–exit sites and, hence, linker histone location within the fibers. In zigzag arrangements, however, the location and orientation of the linker entry–exit sites with respect to the fiber axis are independent of linker DNA length. These sites, with their bound linker histones, face toward the fiber interior, in accordance with neutron-scattering data (63).

Chromatin Topology and DNA Supercoiling. A long-standing problem in the understanding of chromatin architecture has been the absence of an increase in negative superhelicity (or change in linking number, ΔLk) that would be expected from the supercoiling of linker DNA segments in geometries such as solenoids (64, 65). It was suggested by Crick (66) that this apparent paradox may originate from an incomplete understanding of the linker DNA path. The stem motif, now seen to be ubiquitous in a broad range of native chromatins as well as in reconstituted mononucleosomes containing linker histones on linear and minicircle templates (39, 42), can accommodate different linker DNA configurations with correspondingly different ΔLk values (Fig. 3*d*). The case in which the entering and exiting linker DNA segments do not "cross" (Fig. 3*d Upper Right*) is particularly intriguing since the addition (or removal) of linker histone is topologically neutral (42). An important consequence, both for structure and function, is that dramatic changes in chromatin compaction (e.g., from an extended nucleosomal array to a compact chromosomal loop) may occur without a perturbation in topology.

Different levels of chromatin compaction are present in the nucleus and correlate with the degree of transcriptional activation or repression (7, 18, 67, 68). The complete continuum, from decondensed to fully compact, "silenced" chromatin, is compatible with the conserved topological framework of the 3D zigzag of nucleosomes and linker DNA.

The conformation of chromatin, revealed here by EC-M, derives from the interplay of many factors including the ionic milieu, linker histones, and the N termini of the core histones. Determining the precise locations in nucleosomal arrays of these histone domains, which have been inaccessible to x-ray studies (9), is an important future goal.

We thank Ms. Tatiana Nikitina for expert technical assistance. This work was supported by National Institutes of Health Grants GM43786 to C.L.W. and GM45916 to J.C.H., and Deutsche Forschungsgemeinschaft Grant Ty2/4-1,2. The Central Microscopy Facility at the University of Massachusetts, Amherst, is supported in part by National Science Foundation Grants BIR-9419676 and BIR-9419676.

1. van Holde, K. E. (1988) *Chromatin* (Springer, New York).
2. Wolffe, A. P. (1995) *Chromatin Structure and Function* (Academic, London), 2nd Ed.
3. Thoma, F., Koller, T. & Klug, A. (1979) *J. Cell Biol.* **83,** 403–427.
4. Widom, J. (1989) *Annu. Rev. Biophys. Biophys. Chem.* **18,** 365–395.
5. van Holde, K. E. & Zlatanova, J. (1995) *J. Biol. Chem.* **270,** 8373–8376.
6. Woodcock, C. L. & Horowitz, R. A. (1995) *Trends Cell Biol.* **5,** 272–277.
7. Fletcher, T. M. & Hansen, J. C. (1996) *Crit. Rev. Eukaryotic Gene Expression* **6,** 149–188.
8. Arents, G. & Moudrianakis, E. N. (1993) *Proc. Natl. Acad. Sci. USA* **90,** 10489–10493.
9. Luger, K., Mader, A. W., Richmond, R. K., Sargent, D. F. & Richmond, T. J. (1997) *Nature (London)* **389,** 251–260.
10. Felsenfeld, G. (1992) *Nature (London)* **355,** 219–224.
11. van Holde, K. E. (1993) *Nature (London)* **362,** 111–112.
12. Turner, B. M. (1991) *J. Cell Sci.* **99,** 13–20.
13. Workman, J. & Buchman, A. R. (1993) *Trends Biochem. Sci.* **18,** 90–95.
14. Wolffe, A. P. (1994) *Cell* **77,** 13–16.
15. Wolffe, A. P. (1994) *Trends Biochem. Sci.* **19,** 240–244.
16. Wolffe, A. P. (1994) *Curr. Opin. Genet. Dev.* **4,** 245–254.
17. Paranjape, S. M., Kamakaka, R. T. & Kadonaga, J. T. (1994) *Annu. Rev. Biochem.* **63,** 265–297.
18. Kingston, R. E., Bunker, C. A. & Imbalzano, A. (1996) *Genes Dev.* **10,** 905–920.
19. Svaren, J. & Horz, W. (1993) *Curr. Opin. Genet. Dev.* **3,** 52–56.
20. Widom, J. (1986) *J. Mol. Biol.* **190,** 411–424.
21. Clark, D. J. & Kimura, T. (1990) *J. Mol. Biol.* **211,** 883–896.
22. Allan, J., Harborne, N., Rau, D. C. & Gould, H. (1982) *J. Cell Biol.* **93,** 285–297.
23. Garcia-Ramirez, M., Dong, F. & Ausio, J. (1992) *J. Biol. Chem.* **267,** 19587–19595.
24. Fletcher, T. M. & Hansen, J. C. (1995) *J. Biol. Chem.* **270,** 25359–25362.
25. Schwarz, P. M., Fletcher, T. M., Felthauser, A. & Hansen, J. C. (1996) *Biochemistry* **35,** 4009–4015.
26. Allan, J., Mitchell, T., Harborne, N., Boehm, L. & Crane-Robinson, C. (1986) *J. Mol. Biol.* **187,** 591–601.
27. Dubochet, J., Adrian, M., Chang, J. J., Homo, J. C., Lepault, J., McDowall, A. W. & Schultz, P. (1988) *Q. Rev. Biophys.* **21,** 129–228.
28. Ruiz, T., Erk, I. & Lepault, J. (1994) *Biol. Cell* **80,** 203–210.
29. Bednar, J., Horowitz, R. A., Dubochet, J. & Woodcock, C. L. (1995) *J. Cell Biol.* **131,** 1365–1376.
30. Simpson, R. T., Thoma, F. & Brubaker, J. (1985) *Cell* **42,** 799–808.
31. Hansen, J. C., Ausio, J., Stanik, V. H. & van Holde, K. E. (1989) *Biochemistry* **28,** 9129–9136.
32. Schwarz, P. M. & Hansen, J. C. (1994) *J. Biol. Chem.* **269,** 16284–16289.
33. Woodcock, C. L. & Horowitz, R. A. (1997) *Methods* **12,** 84–95.
34. Horowitz, R. A., Koster, A. B., Walz, J. & Woodcock, C. L. (1997) *J. Struct. Biol.* **120,** 353–362.
35. Dubochet, J., Bednar, J., Furrer, P., Stasiak, A. Z. & Bolshoy, A. A. (1994) *Nat. Struct. Biol.* **1,** 361–363.
36. Leuba, S. H., Yang, G., Robert, C., Samori, K., van Holde, K., Zlatnova, J. & Bustamente, C. (1994) *Proc. Natl. Acad. Sci. USA* **91,** 11621–11625.
37. Woodcock, C. L., Frado, L.-L. Y. & Rattner, J. B. (1984) *J. Cell Biol.* **99,** 42–52.
38. Carruthers, L. M., Bednar, J., Woodcock, C. L. & Hansen, J. C. (1998) *Biochemistry* **37,** 14776–14787.
39. Hamiche, A., Schultz, P., Ramakrishnan, V., Oudet, P. & Prunell, A. (1996) *J. Mol. Biol.* **257,** 30–41.
40. Furrer, P., Bednar, J., Dubochet, J., Hamiche, A. & Prunell, A. (1995) *J. Struct. Biol.* **114,** 177–183.
41. Zlatanova, J., Leuba, S. H. & van Holde, K. (1998) *Biophys. J.* **74,** 2554–2566.
42. Prunell, A. (1988) *Biophys. J.* **74,** 2531–2544.
43. Crane-Robinson, C. (1997) *Trends Biochem. Sci.* **22,** 75–77.
44. Wolffe, A. P., Khochbin, S. & Dimitrov, S. (1997) *BioEssays* **19,** 249–255.
45. Losa, R., Thoma, F. & Koller, T. (1984) *J. Mol. Biol.* **175,** 529–551.
46. Simpson, R. T. (1978) *Biochemistry* **17,** 5524–5531.
47. Meersseman, G., Pennings, S. & Bradbury, E. M. (1991) *J. Mol. Biol.* **220,** 89–100.
48. Bates, D. L. & Thomas, J. O. (1981) *Nucleic Acids Res.* **9,** 5883–5894.
49. Staynov, D. Z. (1983) *Int. J. Biol. Macromol.* **5,** 3–9.
50. Bordas, J., Perez-Grau, L., Koch, M. H. J., Vega, M. C. & Nave, C. (1986) *Eur J. Biophys.* **13,** 175–185.
51. Williams, S. P., Athey, B. D., Muglia, L. J., Schappe, R. S., Gough, A. H. & Langmore, J. P. (1986) *Biophys. J.* **49,** 233–248.
52. Woodcock, C. L., Grigoryev, S. A., Horowitz, R. A. & Whitaker, N. (1993) *Proc. Natl. Acad. Sci. USA* **90,** 9021–9025.
53. Kubista, M., Hagmar, P., Nielsen, P. E. & Norden, B. (1990) *J. Biomol. Struct. Dyn.* **8,** 37–54.
54. Pennings, S., Meersseman, G. & Bradbury, E. M. (1994) *Proc. Natl. Acad. Sci. USA* **91,** 10275–10279.
55. O'Neill, T. E., Meersseman, G., Pennings, S. & Bradbury, E. M. (1995) *Nucleic Acids Res.* **23,** 1075–1082.
56. Gerchman, S. E. & Ramakrishnan, V. (1987) *Proc. Natl. Acad. Sci. USA* **84,** 7802–7806.
57. Fletcher, T. M., Serwer, P. & Hansen, J. C. (1994) *Biochemistry* **28,** 10859–10863.
58. Koster, A. J., Chen, H., Sedat, J. W. & Agard, D. A. (1992) *Ultramicroscopy* **46,** 207–227.
59. Tse, C. & Hansen, J. C. (1997) *Biochemistry* **36,** 11381–11388.
60. Horowitz, R. A., Agard, D. A., Sedat, J. W. & Woodcock, C. L. (1994) *J. Cell Biol.* **125,** 1–10.
61. Widom, J. (1992) *Proc. Natl. Acad. Sci. USA* **89,** 1095–1099.
62. Butler, P. J. G. (1984) *EMBO J.* **3,** 2599–2604.
63. Graziano, V., Gerchman, S. E., Schneider, D. K. & Ramakrishnan, V. (1994) *Nature (London)* **368,** 351–354.
64. Germond, J. E., Hirt, B., Oudet, P., Gross-Ballard, M. & Chambon, P. (1975) *Proc. Natl. Acad. Sci. USA* **72,** 1843–1847.
65. Keller, W. Muller, U., Eicken, I., Wendel, I. & Zentgraf, H. (1977) *Symp. Quant. Biol.* **42,** 227–244.
66. Crick, F. H. C. (1976) *Proc. Natl. Acad. Sci. USA* **73,** 2639–2643.
67. Weintraub, H. (1985) *Cell* **42,** 705–711.
68. Wallrath, L. L. & Elgin, S. C. R. (1995) *Genes Dev.* **9,** 1263–1277.